AIAA Guidance, Navigation and Control Conference and Exhibit
18 - 21 August 2008, Honolulu, Hawaii

AIAA 2008-7459

Comparison between Three Spiraling Ballistic Missile State Estimators

Jinwhan Kim*, S. S. Vaddi*, and P. K. Menon†
Optimal Synthesis Inc., Los Altos, CA 94022

and

E. J. Ohlmeyer‡
Naval surface Warfare Center, Dahlgren, VA 22448

During the reentry to the atmosphere, certain ballistic missiles are known to undergo violent spiraling motions induced by aerodynamic resonance between roll and yaw/pitch modes. Successful interception of such a spiraling target is critically dependent on the performance of the target state estimator. Strong nonlinearities involved in the system dynamics and measurement equations together with sensor noise make this a challenging estimation task. The performance of the Extended Kalman Filter, the Unscented Kalman Filter, and the Particle Filter designed for this estimation problem is compared in this paper. Additionally, a hybrid Rao-Blackwellized Particle Filter approach combining the Extended Kalman Filter and the Particle Filter is also considered. Simulation results are provided to support the conclusions from the present study.

Nomenclature

X_T	=	North position of the target
Y_T	=	East position of the target
Z_T	=	Down position of the target
X_m	=	North position of the missile
Y_m	=	East position of the missile
Z_m	=	Down position of the missile
$G_{x,y,z}$	=	Gravitational acceleration components of the target
$A_{x,y,z}$	=	Aerodynamic acceleration components of the target
ω	=	Spiraling frequency of the target
φ	=	Aerodynamic roll angle of the target
c_0, c_1	=	Constants of atmospheric density model
V_T	=	Velocity of the target
R_E	=	Radius of the Earth
γ_T	=	Flight path angle of the target
χ_T	=	Heading angle of the target
C_D	=	Drag coefficient of the target
C_N	=	Normal force coefficient of the target
m_T	=	Mass of the target

* Research Scientist, 95 First Street, Suite 240, Member AIAA.
† Chief Scientist, 95 First Street, Suite 240, Associate Fellow AIAA.
‡ Principal Guidance and Control Engineer, 17320 Dahlgren Road, Associate Fellow AIAA.

S_{ref} = Reference area of the target

C_{D_m} = Modified drag coefficient of the target

C_{N_m} = Modified normal force coefficient of the target

Z_1, Z_2 = Harmonic oscillator states

λ_y, λ_z = Line of sight angles with respect to the target

$\dot{\lambda}_y, \dot{\lambda}_z$ = Line of sight angular rates

R = Relative range with respect to the target

$\dot{R}$ = Relative range rate with respect to the target

$\mathbf{x}$ = System dynamics state vector

$\hat{\mathbf{x}}_k^{(-)}$ = Predicted state estimate vector

$\hat{\mathbf{x}}_k^{(+)}$ = Updated state estimate vector

$\mathbf{z}$ = Measurement state vector

$\mathbf{n}_\mathbf{x}$ = Disturbance noise vector

$\mathbf{n}_\mathbf{z}$ = Measurement noise vector

$\mathbf{f}(\cdot,\cdot)$ = System dynamics function

$\mathbf{h}(\cdot)$ = Measurement function

F = Jacobian of the system dynamics vector ($=\partial\mathbf{f}/\partial\mathbf{x}$)

H = Jacobian of the measurement vector ($=\partial\mathbf{h}/\partial\mathbf{x}$)

Q_x = Error covariance of the process noise

R_z = Error covariance of the measurement noise

$P_k^{(-)}$ = Error covariance of the predicted state estimates

$P_k^{(+)}$ = Error covariance of the updated state estimates

K = Kalman gain matrix

I. Introduction

Motions of a non-separating tactical ballistic missile (TBM) during reentry are known to be highly complex. During exoatmospheric flight the missile may undergo transient motions of precession and nutation. As the missile reenters the atmosphere, these transient motions vanish due to increasing aerodynamic forces, but a rolling motion with trim can develop due to the configurational asymmetry or manufacturing tolerances. If the rolling motion grows and its frequency approaches the missile's natural pitch frequency, the missile exhibits a violent spiraling motion caused by the resonance between pitch and roll modes, called “roll resonance”. This violent spiraling behavior of the target makes the interception task challenging.

For the formulation of filter system dynamics, the motion of the target missile is modeled as a point-mass object, and its motion states are estimated based on bearing/range measurements. In order to improve the overall filter performance, parameters which represent spiral motion of the target are introduced into the system dynamics as additional system states to be estimated. This state augmentation leads to a dual estimation problem which involves both state and parameter estimation tasks. The dual estimation formulation is inherently a highly nonlinear problem due to nonlinear aerodynamic characteristics and nonlinear harmonic motion properties.

Various nonlinear filtering techniques are applicable to this interception problem. Previous research efforts have discussed the performance comparison between nonlinear filters for the interception of a non-spiraling target, however no consensus about the best approach appears to have been reached [1, 2, 3].

In this paper, three different nonlinear filters, 1) Extended Kalman Filter (EKF), 2) Unscented Kalman Filter (UKF), and 3) Particle Filter (PF) are formulated to the spiraling target state estimation problem. The performance of these three filters is compared through a series of numerical simulations, and the detailed performance analysis results are presented. In particular, for the performance analysis, the filter characteristics and performance are carefully examined during the time propagation process and the measurement update process. Additionally, the use of the Rao-Blackwellized Particle Filter (RBPF), which is a hybrid approach combining the EKF and PF, is also discussed.

Related work on spiraling target model analysis and nonlinear filtering is briefly described in Section II. The mathematical model for representing nonlinear target dynamics and the associated filter formulations are presented in Section III. The three nonlinear filtering techniques are described in Section IV, and the performance analysis of the filters during the propagation and measurement update steps is discussed in V. The simulation results with a comprehensive performance comparison between the three filters are presented in Section VI. Finally, the conclusions from the present research are given in Section VII.

II. Related Work

Stability analysis of projectiles such as missiles, shells or bullets has long been an important problem in classical dynamics, and considerable research attention has been focused on dynamic modeling of the projectiles including re-entry of ballistic missiles. Angular motions of symmetric and slightly asymmetric missiles were studied and the associated criteria were presented by Murphy in References 5 and 6. The ballistic missile flight behavior including anomalous roll behavior that leads to coning instabilities was described in terms of the classical Euler angle coordinate system by Platus in References 7 and 8. Chadwick and Zarchan pointed out that the rolling velocity of a non-separating ballistic missile during reentry caused by configurational asymmetries may result in severe spiraling motions at the missile's natural pitch frequency called "roll resonance" or "roll lock-in" [9].

Guidance laws for weaving targets have been applied to the interception of spiraling targets, with the assumption that the target motion can be approximated as a sinusoidal function [10]. The use of a bank of linear Kalman filters was proposed for improving the interception performance against a weaving or spiraling target in Reference 11. An EKF-based formulation with an integrated guidance/control algorithm was proposed by introducing additional parameter states to be estimated for describing spiraling motion in Reference 12.

Apart from the EKF, other nonlinear estimation techniques are also applicable to the missile interception problem. Various nonlinear filters have been applied to non-spiraling missile tracking and their performance comparison studies have been performed. For instance, in Reference 1, Farina et al. claimed that the simulation results favor the EKF over other filters such as the statistical linearization, the unscented Kalman filter, and the particle filter (PF). Saulson and Chang concluded that the central difference filter (CDF), which is very similar to the UKF, demonstrated relatively consistent stability compared to the EKF [2]. Zhao et al. claimed that the Linear Minimum Mean Square Error (LMMSE) filter outperforms other nonlinear filters [3]. In fact, no definite consensus was reached by the above mentioned comparison studies.

Present research focuses on the motion state-parameter estimation of a spiraling target. For the performance comparison, three commonly used nonlinear filters, namely the EKF, UKF, and PF are selected. Moreover, a hybrid Rao-Blackwellized Particle Filter (RBPF) that combines the EKF and PF is also considered. The RBPF is known to be an effective approach for systems with mixed linear/nonlinear states [13,14].

III. Target Modeling

A. Equations of Motion

A complete description of spiral dynamics during the reentry may require a full 6-DOF model. However, the spiral motion near the resonance frequency can be represented as a steady harmonic motion with reasonable accuracy [9]. Based on this steady state approximation, a simplified 3-D point-mass model with rotating lift force terms is used for describing the target missile's motion [12]. Acceleration of the target is the sum of gravitational and aerodynamic components. Equations of motion of the target in an inertial frame of reference fixed to the surface of the Earth are as follows:

$$\ddot{X}_T = G_x + A_x \tag{1}$$

$$\ddot{Y}_T = G_y + A_y \tag{2}$$

$$\ddot{Z}_T = G_z + A_z \tag{3}$$

Gravitational acceleration of the target can be modeled using an inverse square law model described by the following equation:

$$\begin{bmatrix} G_x \\ G_y \\ G_z \end{bmatrix} = -\frac{\mu}{\left[X_t^2 + Y_T^2 + (Z_T - R_e)^2 \right]^{3/2}} \begin{bmatrix} X_T \\ Y_T \\ Z_T - R_e \end{bmatrix} \tag{4}$$

Aerodynamic forces acting on the target can be divided into two major components: 1) drag acting along the direction of the velocity vector, and 2) normal force acting in a plane perpendicular to the velocity vector. Spiraling motion is caused by the normal forces. Magnitudes of the two aerodynamic force components are dependent on the drag coefficient and normal force coefficient apart from the dynamic pressure. In general, the aerodynamic coefficients vary with Mach number, altitude, angle of attack and angle of side-slip. However, these are assumed to be constant in this paper. Spiraling motion can be simulated by a constant magnitude normal acceleration vector rotating at a constant rate in the plane normal to the velocity vector. Aerodynamic acceleration components resulting from drag and rotating normal acceleration can be represented by:

$$\begin{bmatrix} A_x \\ A_y \\ A_z \end{bmatrix} = \begin{bmatrix} \cos\gamma_T \cos\chi_T & -\sin\chi_T & \sin\gamma_T \cos\chi_T \\ \cos\gamma_T \sin\chi_T & \cos\chi_T & \sin\gamma_T \sin\chi_T \\ -\sin\gamma_T & 0 & \cos\gamma_T \end{bmatrix} \begin{bmatrix} -\dfrac{\rho V_T^2 S_{ref} C_D}{2m_T} \\ \dfrac{\rho V_T^2 S_{ref} C_N}{2m_T} \cos\varphi \\ \dfrac{\rho V_T^2 S_{ref} C_N}{2m_T} \sin\varphi \end{bmatrix} \tag{5}$$

In Equation (5), φ is the rolling angle which is a function of time, and its time derivative is the rolling frequency.

$$\dot{\varphi} = \omega \tag{6}$$

The variable ω is the rolling frequency, assumed to be equal to the steady state roll resonance frequency.

B. Model for Estimator Design

The dynamic model described in the previous section consists of motion states such as position and velocity and various parameters such as the aerodynamic coefficients, mass of the target, reference area, phase and spiral frequency. It is not possible to uniquely estimate all the constants using the sensor measurements that are determined by position and velocity alone. Therefore, modifications are sought to the target model described in the previous section to achieve observability as well as eliminate the explicit dependence of time. The following grouping of terms is used to reduce the number of unknowns:

$$C_{Dm} = \frac{S_{ref} C_D}{m_T} \tag{7}$$

$$C_{Nm} = \frac{S_{ref} C_N}{m_T} \tag{8}$$

Two new state components Z_1 and Z_2 are defined to avoid the explicit appearance of time in the trigonometric expressions:

$$Z_1 = C_{Nm} \cos\varphi \tag{9}$$

$$Z_2 = C_{Nm} \sin\varphi \tag{10}$$

Atmospheric density is modeled as an exponential function of altitude as:

$$\rho = c_0 e^{c_1 Z_T} \tag{11}$$

where $c_0 = 0.0038$ and $c_1 = 0.047407\text{e-}3$.

With the above modifications the augmented filter state vector to be estimated can be represented as

$$\mathbf{x} = \begin{bmatrix} X_T & Y_T & Z_T & \dot{X}_T & \dot{Y}_T & \dot{Z}_T & Z_1 & Z_2 & C_{Dm} & \omega \end{bmatrix}^T \tag{12}$$

The associated dynamic model is given by the following equations.

$$\begin{bmatrix} \ddot{X}_T \\ \ddot{Y}_T \\ \ddot{Z}_T \end{bmatrix} = -\frac{\mu}{\left[X_t^2 + Y_T^2 + (Z_T - R_e)^2 \right]^{3/2}} \begin{bmatrix} X_T \\ Y_T \\ Z_T - R_e \end{bmatrix} + \frac{c_0 e^{c_z Z_T} V_T^2}{2} T_{W,I}(\gamma_T, \chi_T) \begin{bmatrix} -C_{Dm} \\ Z_1 \\ Z_2 \end{bmatrix} \tag{13}$$

Dynamics of Z_1 and Z_2 is modeled by a harmonic oscillator.

$$\begin{bmatrix} \dot{Z}_1 \\ \dot{Z}_2 \end{bmatrix} = \begin{bmatrix} 0 & -\omega \\ \omega & 0 \end{bmatrix} \begin{bmatrix} Z_1 \\ Z_2 \end{bmatrix} \tag{14}$$

$$\dot{C}_{Dm} = 0 \tag{15}$$

$$\dot{\omega} = 0 \tag{16}$$

Note that the modified drag coefficient and the spiral frequency are modeled as piecewise constants. However moderate time variations of these parameters can also be accommodated by introducing non-zero process noise terms.

C. Measurement Model

It is assumed that the measurement vector consists of the line of sight angles, line of sight angular rates, relative range, and range rate. The measurement vector is:

$$\mathbf{z} = \begin{bmatrix} \lambda_y & \lambda_z & \dot{\lambda}_y & \dot{\lambda}_z & R & \dot{R} \end{bmatrix}^T \tag{17}$$

These measurements are available with respect to the missile platform. The line of sight angles are defined as:

$$\lambda_y = tan^{-1}\left(\frac{Y_T - Y_m}{X_T - X_m} \right) = tan^{-1}\left(\frac{\Delta Y}{\Delta X} \right) \tag{18}$$

$$\lambda_z = tan^{-1}\left(\frac{Z_T - Z_m}{X_T - X_m} \right) = tan^{-1}\left(\frac{\Delta Z}{\Delta X} \right) \tag{19}$$

X_m, Y_m, and Z_m are components of the interceptor position vector, assumed to be known. Expressions for the line-of-sight rates can be obtained by differentiating the above expressions:

$$\dot{\lambda}_y = \frac{\Delta X \Delta \dot{Y} - \Delta Y \Delta \dot{X}}{\Delta X^2 + \Delta Y^2} \tag{20}$$

$$\dot{\lambda}_z = \frac{\Delta X \Delta \dot{Z} - \Delta Z \Delta \dot{X}}{\Delta X^2 + \Delta Z^2} \tag{21}$$

Range and range rate expressions are given

$$R = \sqrt{\Delta X^2 + \Delta Y^2 + \Delta Z^2} \tag{22}$$

$$\dot{R} = \frac{\Delta X \Delta \dot{X} + \Delta Y \Delta \dot{Y} + \Delta Z \Delta \dot{Z}}{\sqrt{\Delta X^2 + \Delta Y^2 + \Delta Z^2}} \tag{23}$$

IV. Nonlinear Filters

The target dynamics given in the foregoing is nonlinear. In Reference 12, the EKF methodology was applied to this nonlinear estimation problem, and satisfactory results were obtained for several interception scenarios. In this paper, the study is extended to a comparative evaluation of emerging nonlinear filter formulations. Specifically, the Unscented Kalman filter (UKF) and the Particle Filter (PF) are selected for performance comparison with the EKF. The UKF is chosen because it is one of the most common filters among the class of linear regression Kalman filters and is known to perform better than EKF in many nonlinear estimation problems. The PF is selected because of its

versatility and flexibility in dealing with highly nonlinear systems with non-Gaussian uncertainties at the cost of increased computational demand.

The system dynamics and measurement equation of the target tracking problem can be rewritten in the standard state-space form as follows:

$$\begin{aligned} \dot{\mathbf{x}} &= \mathbf{f}(\mathbf{x},\mathbf{u}) + \mathbf{n}_{\mathbf{x}} \\ \mathbf{z} &= \mathbf{h}(\mathbf{x}) + \mathbf{n}_{\mathbf{z}} \end{aligned} \tag{24}$$

where $\mathbf{n_x}$ and $\mathbf{n_z}$ are Gaussian noise vectors that follow $\mathbf{n_x}$~N(0,Q_x) and $\mathbf{n_z}$~N(0,R_z), respectively. Brief descriptions of the three nonlinear filtering techniques (i.e. EKF, UKF, and PF) in terms of the state-measurement system in (24) follow.

A. Extended Kalman Filter (EKF)

The Extended Kalman Filter is one of the most widely used nonlinear filters in a variety of estimation applications. The filter has been applied to many engineering and scientific applications since it first appeared in the early 60s. In the EKF formulation, the state distribution is approximated by Gaussian random variables, and then propagated along time through the 1st order Taylor series approximation (i.e. linear approximation) of the original nonlinear dynamics/measurement equations [15,16]. The validity of the above approximations (i.e. linearization and/or Gaussian approximation) restricts the use of the EKF, and may cause large errors for systems with high nonlinearity and non-Gaussian noise distributions. However, the EKF continues to be widely used for many practical applications and systems with nonlinearities and non-Gaussian uncertainty properties, mainly due to the computational efficiency and well-established systematic design procedure. The pseudo code of the algorithm reproduced from Reference 20 is presented in Table 1.

Table 1 The Extended Kalman Filter Algorithm [20]

Algorithm Extended_Kalman_Filter $\left(\hat{\mathbf{x}}_{k-1}^{(+)}, P_{k-1}^{(+)}, \mathbf{u}_k, \mathbf{z}_k\right)$

$\hat{\mathbf{x}}_k^{(-)} = \mathbf{f}\left(\hat{\mathbf{x}}_{k-1}^{(+)}, \mathbf{u}_k\right)$

$P_k^{(-)} = FP_{k-1}^{(+)}F^T + Q_x^d$

$K_k = P_k^{(-)}H^T\left(HP_k^{(-)}H^T + R_z^d\right)^{-1}$

$\hat{\mathbf{x}}_k^{(+)} = \hat{\mathbf{x}}_k^{(-)} + K_k\left(\mathbf{z}_k - \mathbf{h}\left(\hat{\mathbf{x}}_k^{(-)}\right)\right)$

$P_k^{(+)} = \left(I - K_k H\right)P_k^{(-)}$

return $\left(\hat{\mathbf{x}}_k^{(+)}, P_k^{(+)}\right)$

B. Unscented Kalman Filter (UKF)

The Unscented Kalman Filter (UKF) uses a sampling approach to overcome the limitation due to the linearization process of the EKF [17]. This bears some superficial resemblance to the Particle Filter (PF) outlined in the next section. Instead of randomly choosing a number of state particles as the PF does, the UKF's particles are carefully selected in a deterministic way to ensure they match a desired mean and covariance for the prior distribution. The selected particles are propagated along time through the system's original nonlinear dynamics, and then again approximated as a Gaussian distribution after the propagation (i.e. unscented transformation). This technique is known to be capable of capturing the posterior mean and covariance accurately to the 3rd order Taylor series expansion [18]. The UKF has recently been applied to a wide class of nonlinear estimation problems, and has been reported to outperform the EKF in many applications.

The UKF is also known as the Sigma-Point Kalman Filter (SPKF). For a system with a dimension of n, $2n$+1 points, called sigma-points, are selected based on a specific rule. Unlike the EKF, no Jacobian matrix calculation is required for the UKF. Thus it is often called a derivative-free filter. It is known that the complexity of the algorithm and overall computational cost of the UKF are almost equivalent to those of the EKF. The UKF algorithm is outlined in Table 2.

Table 2 The Unscented Kalman Filter Algorithm [20]

Algorithm Unscented_Kalman_Filter $\left(\hat{\mathbf{x}}_{k-1}^{(+)}, P_{k-1}^{(+)}, \mathbf{u}_k, \mathbf{z}_k\right)$

$$\chi_{k-1} = \left[\hat{\mathbf{x}}_{k-1}^{(+)} \;,\; \hat{\mathbf{x}}_{k-1}^{(+)} + \sqrt{(n+\lambda)P_{k-1}^{(+)}} \;,\; \hat{\mathbf{x}}_{k-1}^{(+)} - \sqrt{(n+\lambda)P_{k-1}^{(+)}}\right]$$

$$\chi_k^* = \mathbf{f}\left(\chi_{k-1}, \mathbf{u}_k\right)$$

$$\hat{\mathbf{x}}_k^{(-)} = \sum_{i=0}^{2n} w_{m,i}\, \chi_{k,i}^*$$

$$P_k^{(-)} = \sum_{i=0}^{2n} w_{c,i}\left(\chi_{k,i}^* - \hat{\mathbf{x}}_k^{(-)}\right)\left(\chi_{k,i}^* - \hat{\mathbf{x}}_k^{(-)}\right)^T + Q_x^d$$

$$\chi_k = \left[\hat{\mathbf{x}}_k^{(-)} \;,\; \hat{\mathbf{x}}_k^{(-)} + \sqrt{(n+\lambda)P_k^{(-)}} \;,\; \hat{\mathbf{x}}_k^{(-)} - \sqrt{(n+\lambda)P_k^{(-)}}\right]$$

$$\zeta_k = \mathbf{h}\left(\chi_k\right)$$

$$\hat{\mathbf{z}}_k = \sum_{i=0}^{2n} w_{m,i}\, \zeta_{k,i}$$

$$S_k = \sum_{i=0}^{2n} w_{c,i}\left(\zeta_{k,i} - \hat{\mathbf{z}}_{k,i}\right)\left(\zeta_{k,i} - \hat{\mathbf{z}}_{k,i}\right)^T + R_z^d$$

$$P_k^{xz} = \sum_{i=0}^{2n} w_{c,i}\left(\chi_{k,i} - \hat{\mathbf{x}}_{k,i}^{(-)}\right)\left(\zeta_{k,i} - \hat{\mathbf{z}}_{k,i}\right)^T$$

$$K_k = P_k^{xz} S_k^{-1}$$

$$\hat{\mathbf{x}}_k^{(+)} = \hat{\mathbf{x}}_k^{(-)} + K_k\left(\mathbf{z}_k - \hat{\mathbf{z}}_k\right)$$

$$P_k^{(+)} = P_k^{(-)} - K_k S_k K_k^T$$

return $\left(\hat{\mathbf{x}}_k^{(+)}, P_k^{(+)}\right)$

Here n is the state dimension and λ is the sigma-point scaling parameter. The parameter λ and the associated weighting vectors can be determined using the following rules.

$$\lambda = \alpha^2\left(n + \kappa\right) - n \tag{25}$$

$$\begin{aligned} w_{m,0} &= \frac{\lambda}{n+\lambda} \quad , \quad w_{m,i} = \frac{1}{2(n+\lambda)} \quad \text{for} \quad i = 1, \cdots, 2n \\ w_{c,0} &= \frac{\lambda}{n+\lambda} + \left(1 - \alpha^2 + \beta\right) \quad , \quad w_{m,i} = \frac{1}{2(n+\lambda)} \quad \text{for} \quad i = 1, \cdots, 2n \end{aligned} \tag{26}$$

In these equations, α, β and κ are additional scaling parameters [17,18,20].

C. Particle Filter (PF)

Increasing power of onboard computers has made the Particle Filter (PF) attractive in several problems such as nonlinear estimation, machine learning, and parameter identification. The key idea of the PF is to represent the system uncertainty distributions using a cloud of particles instead of the state estimate and error covariance matrix. The PF formulation is based on the Monte-Carlo simulation technique. However the PF incorporates a specific process called resampling, to choose more important high-weighted particles and to discard lower weighted particles. Although the approach taken by the PF may not be mathematically aesthetic, it requires virtually no restrictive assumptions on the system dynamics or uncertainty distributions. Consequently, it often provides good results for highly nonlinear/non-Gaussian systems. In particular, the PF can be much more effective for a system whose uncertainty distribution is not unimodal – the probabilistic distribution has two or more peaks – than the Gaussian filters like the EKF and UKF which approximate any uncertainty as a unimodal Gaussian distribution

function. However, the PF algorithm is computationally intensive, and may not be amenable to real-time application in high-dimensional systems.

Several algorithmic variants of the PF exist. In this paper, a standard PF based on sampling importance resampling (SIR) is used. The algorithm is outlined in Table 3.

Table 3 The Particle Filter Algorithm [20,21]

Algorithm Particle_Filter $\left(\chi_{k-1}^{(+)}, \mathbf{u}_k, \mathbf{z}_k\right)$

$\chi_k^{(-)} = \chi_k^{(+)} = \mathbf{0}$

for $i = 1$ to $n_{particles}$

sample $\hat{\mathbf{x}}_k^i \sim p\left(\hat{\mathbf{x}}_k \mid \hat{\mathbf{x}}_{k-1}, \mathbf{u}_k\right)$

$w_k^i = p\left(\mathbf{z}_k \mid \hat{\mathbf{x}}_k^i\right)$

$\chi_k^{(-)} = \chi_k^{(-)} + \left\langle \hat{\mathbf{x}}_k^i, w_k^i \right\rangle$

end

calculate total weight $W = \sum_{i=1}^{n_{particles}} w_k^i$

for $i = 1$ to $n_{particles}$

normalize $w_k^i := w_k^i / W$

end

for $i = 1$ to $n_{particles}$

draw j with probability $\propto w_k^i$

add $\hat{\mathbf{x}}_k^j$ to $\chi_k^{(+)}$

end

return $\left(\chi_k^{(+)}\right)$

V. Estimation System Performance Analysis

In this section, the validity and utility of applying each of the three filters to the present problem is discussed and demonstrated. Instead of simply comparing the final estimation errors between the filters, the state propagation step and the measurement update step are analyzed separately. This analysis approach is expected to reveal the effectiveness and validity of the simplifying assumptions employed by the EKF and UKF, such as linearization of system dynamics and Gaussian approximation of state/parameter uncertainties. The analysis may also provide supporting evidence to justify the application of the PF to this problem.

A. State propagation process

In order to examine the effectiveness of the state propagation model for each filter through the nonlinear system dynamics of the spiraling target missile, the time propagation results from the EKF, UKF, and PF, all with no measurement update, are compared at several time instances. Specifically, the mean values and covariance matrices are compared. The means and error covariance matrices are directly available for the EKF and UKF. For the PF, its mean and covariance are calculated from the distribution of particles. The comparison allows an assessment of the effectiveness of the uncertainty propagation algorithm through the nonlinear system for each of the filtering techniques. To reiterate, these are the 1st order linear approximation for the EKF, the unscented transformation for the UKF, and Monte-Carlo time propagation for the PF.

Because of the high dimension of the state vector, it is not easy to visualize the full state information altogether. Instead, state pairs of interest are plotted in the 2D plane onto which system states in the high dimensional state-space are projected. The marginal distributions of the target position projected onto the X-Z plane at t=0, t=0.2, t=0.4, and t=0.6 are shown in Figure 1.

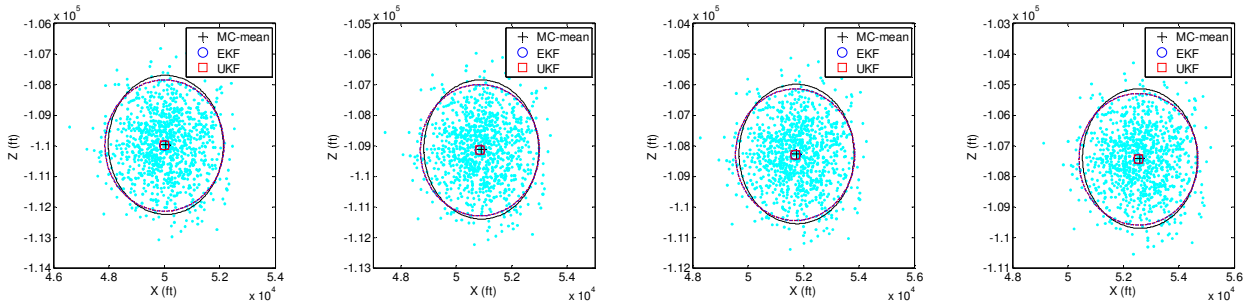

(a) t = 0.0 (sec) (b) t = 0.2 (sec) (c) t = 0.2 (sec) (d) t = 0.6 (sec)

Figure 1 Position Estimates in the X-Z Plane (90% Confidence Ellipses)

In Figure 1, each ellipse around the state estimate represents the confidence ellipse whose size and shape reflect the position estimate uncertainty properties. Specifically, a 90% confidence ellipse means that there is a 90% probability of the actual state existing inside the ellipse. A number of small dots in the figure represent the probabilistic distribution of state estimate by the Monte-Carlo (MC) simulation. The algebraic mean and variance of the particle distribution, which correspond to the mean and variance of the PF with no resampling, are compared with the results by the EKF and UKF.

Initially, the same level of uncertainties in both *X* and *Z* directions are assumed. As shown in Figure 1, this initially circular distribution does not change much over the simulation time period. Small differences between the EKF, UKF, and the Gaussian approximation of MC particles can be seen, and the particle distribution maintains its Gaussian distribution shape. Both the EKF and UKF satisfactorily approximate the distributions of MC particles.

The same analysis is carried out for the parameters Z_1 and Z_2 associated with the harmonic spiraling motion. The results are shown in Figure 2.

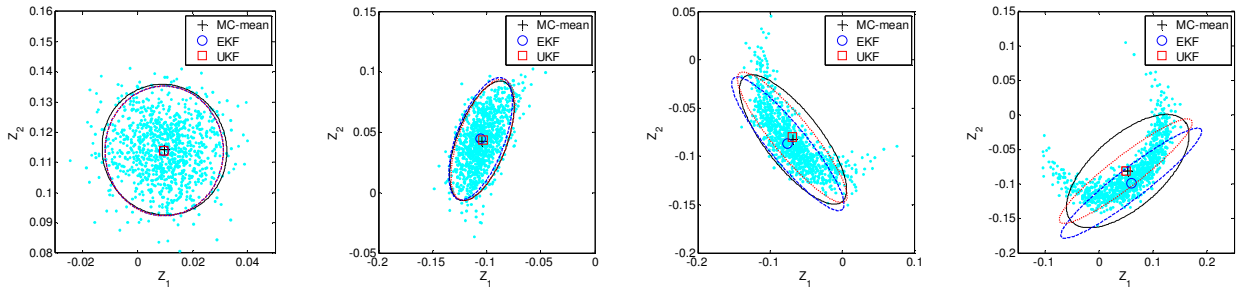

(a) t = 0.0 (sec) (b) t = 0.2 (sec) (c) t = 0.2 (sec) (d) t = 0.6 (sec)

Figure 2 State Estimates for Harmonic Motion (90% Confidence Ellipses)

Unlike the previous case, the distribution in the Z_1-Z_2 plane is noticeably distorted as the system dynamics propagates along time. This is thought to be caused by the nonlinearity of the parameter states in the system dynamics. The initial Gaussian distribution quickly changes into a non-Gaussian distribution as MC particles propagate through the nonlinear system dynamics model. The resulting distribution can effectively be represented by MC particles. The EKF and UKF do not perform as well as the MC particles in dealing with non-Gaussian uncertainty. However they still show fairly acceptable performance. Note that the state estimate by the UKF stays a little closer to the algebraic mean of MC state particles than the EKF. This partially supports the claim that the UKF may show better performance than the EKF in dealing with highly nonlinear systems.

B. Measurement update process

Performance of the three estimators during the measurement update process is next examined. Measurement nonlinearities of the present problem are mostly due to the use of polar coordinates. The system dynamics model uses Cartesian coordinates, however sensor measurements are provided in the form of range and bearing in polar coordinates. To fuse measurement information with the prior estimate, nonlinear transformation between the two coordinate systems is needed.

However, unlike the previous case for the time propagation process, it is not straightforward to demonstrate the performance difference between the three filters during the measurement process. Here, the means and variances of the EKF and UKF are compared and shown in 2-D plots, and MC particles based on the distribution of the currently

available measurement are plotted on top of them. Figure 3 shows numerical simulation results with different initial range estimates to the target and different initial position uncertainties. The measurement distribution to be fused with the prior estimates by the EKF and UKF is plotted as a point cloud in each figure, which is Gaussian in polar coordinates. The 90% confidence ellipses for the EKF and UKF that represent the posterior belief of the target position are shown as well. The plots are captured at t = 50 (ms).

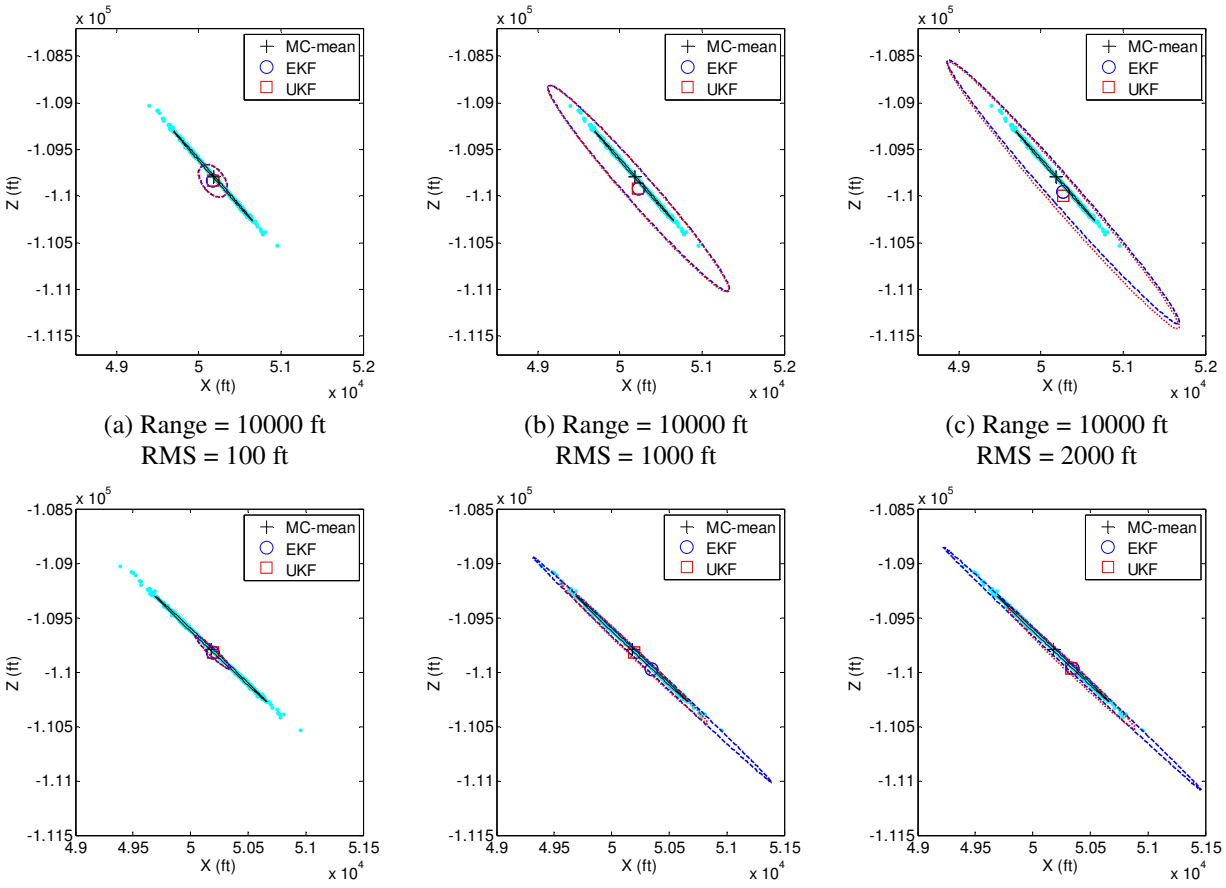

(a) Range = 10000 ft
RMS = 100 ft

(b) Range = 10000 ft
RMS = 1000 ft

(c) Range = 10000 ft
RMS = 2000 ft

(d) Range = 2000 ft
RMS = 100 ft

(e) Range = 2000 ft
RMS = 1000 ft

(f) Range = 2000 ft
RMS = 2000 ft

Figure 3 State Estimate in the X-Z plane

As seen from the above figures, the EKF and UKF show equally satisfactory performance and no significant difference between them can be found. The UKF is known to provide better and more reliable performance than the EKF for the relative position estimation using bearing-only measurements within a small range[19]. However performance advantage in using the UKF is not noticeable for the present system possibly due to the availability of range measurements or perhaps due to the excellent performance provided by the EKF.

The PF performance during the measurement update process is not explicitly shown in Figure 3. In fact, the main advantage of using the PF for the measurement update step is its ability to deal with non-Gaussian measurement noise. The PF is known to outperform other filters, particularly when the sensor noise distribution is far from the Gaussian distribution and if the computational effort is not a limiting factor. However, Gaussian distributions are assumed for the measurement noise uncertainty in the present study. In general, the sensor errors in range and bearing can be well approximated by the Gaussian distribution. Consequently, the advantage of using the PF in terms of measurement update is not expected to be as apparent as in the time propagation step.

VI. Filter Performance Comparison in Simulations

The EKF, UKF and PF are applied to the tracking problem of a ballistic target undergoing a spiraling motion. In particular, three different PF's with 100, 1000 and 10000 particles are used for evaluating the feasibility of applying the PF to the present application. The parameter settings assumed for the simulations are as in Table 4 and Table 5.

Table 4 Initial Uncertainty Settings

	σ_X (ft)	σ_Y (ft)	σ_Z (ft)	$\sigma_{\dot{X}}$ (ft/s)	$\sigma_{\dot{Y}}$ (ft/s)	$\sigma_{\dot{Z}}$ (ft/s)	σ_{Z_1} (ft^2/lb)	σ_{Z_2} (ft^2/lb)	$\sigma_{C_{Dm}}$ (ft^2/lb)	σ_ω (1/s)
Std. Deviation	1.0e3	1.0e3	1.0e3	1.0e2	1.0e2	1.0e2	1.0e-2	1.0e-2	1.0e-3	1.0

Table 5 Measurement Uncertainty Settings

	λ_x (rad)	λ_y (rad)	$\dot{\lambda}_x$ (rad/s)	$\dot{\lambda}_y$ (rad/s)	R (ft)	$\dot{R}$ (ft/s)
Measurement Noise	5.0e-4	5.0e-4	5.0e-3	5.0e-3	1.0e2	1.0e1

A series of simulations with various target engagement scenarios were carried out. Figure 4 shows the error trajectories for the harmonic oscillator parameter states, and compares the estimation performance of the five different filters based on the three filtering techniques. The harmonic oscillator parameter states are directly associated with the spiraling motion of the target. The estimation of these parameters is expected to be particularly challenging due to their nonlinearities and time-varying characteristics.

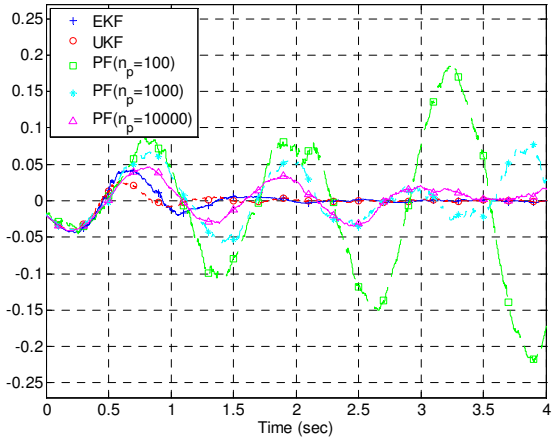

(a) Error in the harmonic oscillator state, Z_1

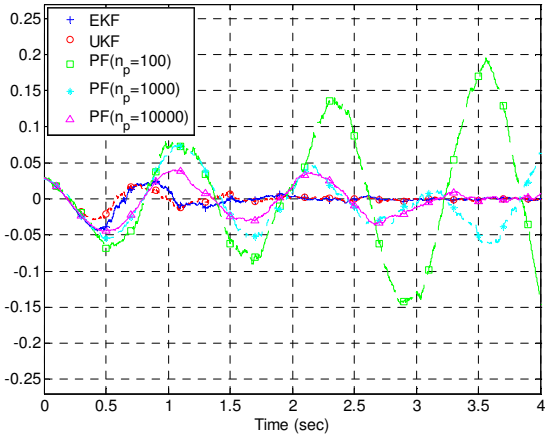

(b) Error in the harmonic oscillator state, Z_2

Figure 4 Error Trajectories for Nonlinear Parameter States by the EKF, UKF, and PF's

Both EKF and UKF show quite satisfactory performance. However, large errors are observed in the PF results. The PF estimation errors decrease as the number of particles increases, which confirms the well-known hypothesis that better PF performance can be expected using more particles. However, even 10000 particles are found to be far from enough to achieve comparable performance to the EKF or UKF for the present problem. It is because the present problem has relatively high state dimensions (i.e. $Dim(\mathbf{x}) = 10$) when compared with the state dimension of the typical PF application examples discussed in the literature. The associated computational costs of the simulations are presented in Table 6.

Table 6 Computational Costs

	EKF	UKF	PF (n_p = 100)	PF (n_p = 1000)	PF (n_p = 10000)
Computational Cost (normalized by the EKF cost)	1.0	1.557	9.364	91.46	912.2

In Table 6, all the costs have been normalized by the computational cost of the EKF. The UKF cost is slightly larger than the EKF's, although their algorithms have nearly equivalent complexity. The complexity of the PF grows linearly with the number of particles. A PF with 100 particles runs much faster than 100 EKF's, however the PF of comparable performance to an EKF generally requires a lot more particles.

In order to get a reasonable estimate for the number of particles to achieve acceptable PF performance, a brief feasibility study was performed using a simplified tracking problem. A reduced-order target tracking problem with 2 states was formulated and a number of simulations were performed. Using this simplified problem, efficient pre-tuning of the PF parameters, such as the resampling interval and the uncertainty level of fictitious disturbance, was also carried out, which would critically affect the overall PF performance. This mini feasibility study showed that several hundreds of particles are required to achieve the performance comparable to the EKF for the target tracking problem in 2-D state space. A specific simulation example shown in Figure 5 used 400 particles.

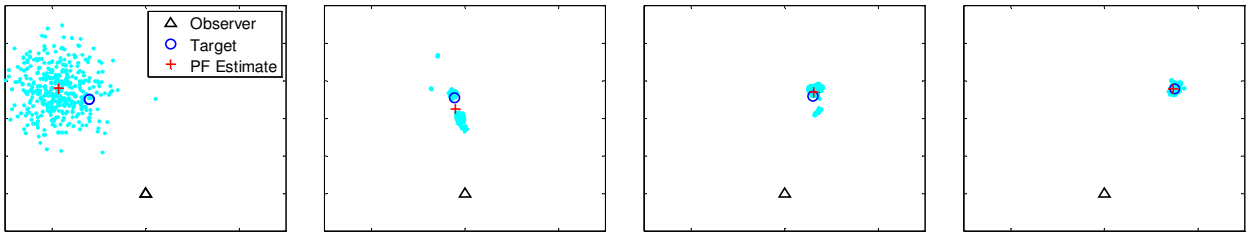

(a) t = 0.0 (b) t = 1.5 (c) t = 3.0 (d) t = 4.5

Figure 5 Particle Filter Simulation for the 2-D Target Tracking Problem (Number of Particles = 400)

Considering that the state-space volume in hyperspace grows exponentially with the state dimension, a naïve PF implementation for the present tracking problem may need an excessively large number of particles, perhaps on the order of tens of billions. The PF performance in terms of both accuracy and computational efficiency might be improved to a certain extent by employing a different variant of the PF with an alternative resampling algorithm. Nevertheless, the PF is expected to be computationally too expensive to be useful for online implementation.

Therefore, it can now be stated that the use of the EKF or UKF is more advantageous than the use of the PF for the current application. More detailed performance comparison between the EKF and UKF is carried out in the following subsection A.

According to the findings so far, any naïve implementation of the PF for the current tracking problem has turned out to be computationally prohibitive and impractical, and the filter performance by the EKF and UKF appears to be quite satisfactory. Thus, it seems that there exists little room for improvement, at least accuracy wise, by exploiting the filtering techniques based on MC simulations. However, it is still worthwhile to investigate other options to reduce the computational requirement of the PF, since the PF enjoys certain advantages that the conventional analytical filters lack. One of the advantages is the filter robustness, particularly against the large initial uncertainty. In fact, for the current application, unlike the position states whose initial estimates are directly available from the sensor measurements, the parameter states are basically hidden internal variables and cannot be easily predicted beforehand. A poor initial guess may result in entrapment in local minima or premature divergence of the EKF or UKF which employs a unimodal Gaussian function for uncertainty representation.

In Subsection B, a hybrid approach for circumventing the computational limitations of the PF is discussed and the associated application results are presented.

A. EKF vs. UKF

The previous performance comparison studies showed that the EKF and UKF outperform the PF considering the available computational resources. The performance between the EKF and UKF are now compared in additional detail. Figure 6-(a) illustrates the present target engagement scenario, and Figure 6-(b), (c) and (d) compare the position state estimates of the spiraling target. Both the EKF and UKF show excellent tracking performance, and very little difference can be observed from the plots.

Figure 7 compares the time histories of the parameter state estimates. Again, both the EKF and UKF successfully converge to the true parameter state values. However, small performance differences are now observable, and the UKF shows slightly better performance than the EKF, supporting the discussion in Section 8.

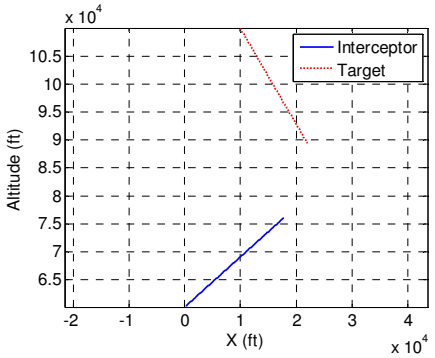

(a) Trajectories of the missile and target

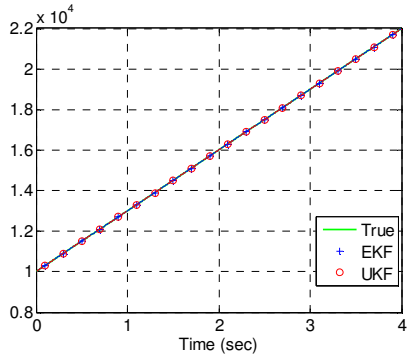

(b) Target position (X_T)

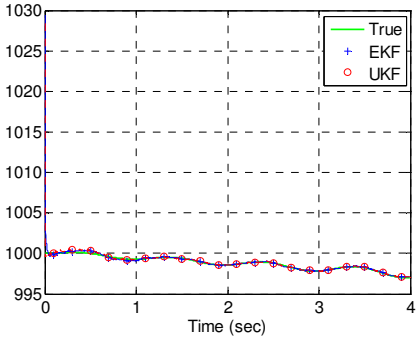

(c) Target position (Y_T)

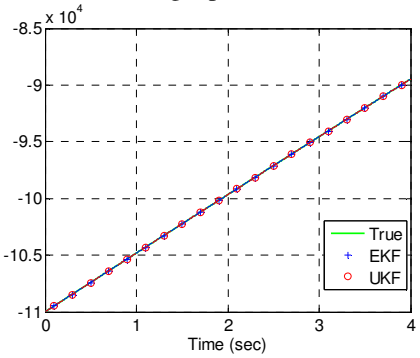

(d) Target position (Z_T)

Figure 6 Position Estimate Comparison

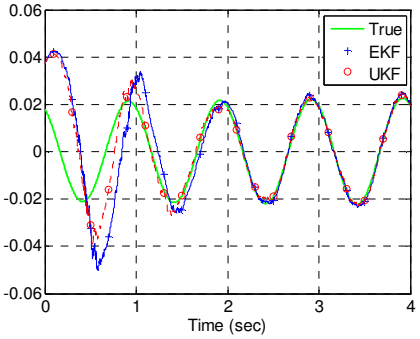

(a) Harmonic oscillation parameter (Z_1)

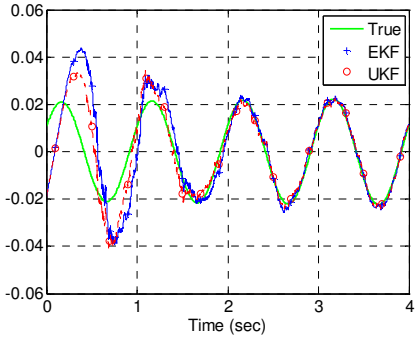

(b) Harmonic oscillation parameter (Z_2)

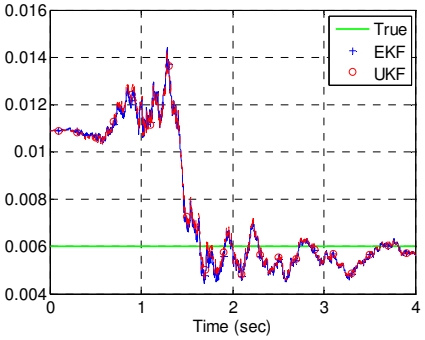

(c) Modified drag coefficient parameter

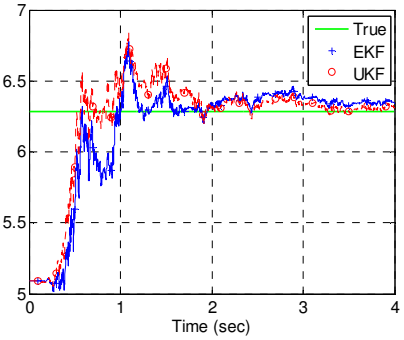

(d) Spiraling frequency parameter

Figure 7 Parameter Estimate Comparison

To verify the performance benefit in using the UKF in more general conditions, Monte-Carlo simulations were performed. The resulting error norm time histories are shown in Figure 8.

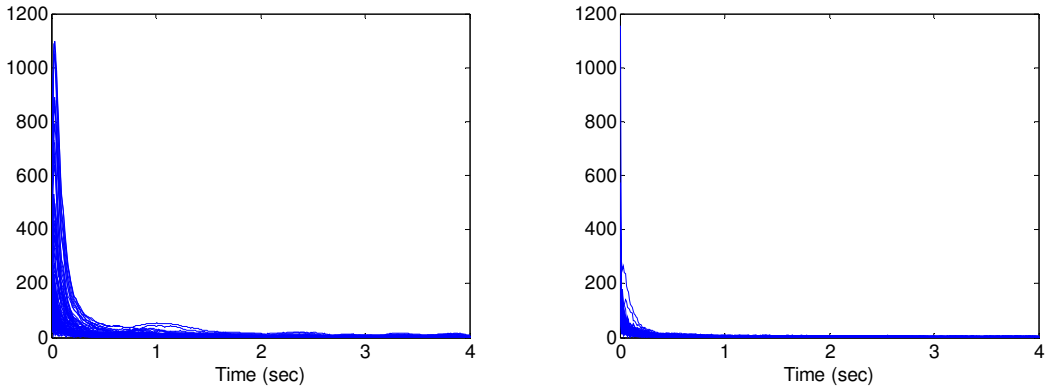

(a) EKF errors (b) UKF errors

Figure 8 Error-Norm Trajectories

The error norm trajectories in the above figure are obtained by performing 100 simulations for each filter. The figure demonstrates that UKF clearly outperforms the EKF. The UKF converges faster and appears to have better stability properties than the EKF. Table 7 presents a quantitative comparison of the results. The UKF provides consistently better performance when compared with the EKF in both the transient and the steady-state phases.

Table 7 Performance Comparison between EKF and UKF

	EKF	UKF	Error Ratio (UKF/EKF)
Mean Error Norm (overall)	6.974	3.198	45.9 %
Mean Error Norm (0 sec ~ 1sec)	13.878	6.335	45.6 %
Mean Error Norm (1sec ~ 4 sec)	0.242	0.105	43.3 %

B. Rao-Blackwellized Particle Filter

The Rao-Blackwellized particle filter (RBPF), also known as the Marginalized Particle Filter, is applied to the present nonlinear estimation problem. This formulation helps avoid the prohibitive computational requirements of the naïve PF implementation.

The RBPF is a hybrid-type filter that combines the particle filter and a filter based on analytical estimation techniques. The filter is known to be effective and efficient for mixed linear/nonlinear systems whose system state vector can be partitioned into two parts which are the linear/Gaussian part ($\mathbf{x}_L$) and the nonlinear/non-Gaussian part ($\mathbf{x}_{NL}$). The key idea of the RBPF can be represented as the following joint probability distribution based on the Bayes' rule.

$$P(\mathbf{x}_L, \mathbf{x}_{NL} \mid \mathbf{z}) = P(\mathbf{x}_L \mid \mathbf{x}_{NL}, \mathbf{z}) P(\mathbf{x}_{NL} \mid \mathbf{z}) \tag{27}$$

Once the second factor on the right hand side of (27) is numerically estimated using the PF, the distribution of $\mathbf{x}_L$ given the distributions of $\mathbf{x}_{NL}$ and $\mathbf{z}$ can be computed using analytical estimation techniques. Thus, the joint probability distribution of $\mathbf{x}_L$ and $\mathbf{x}_{NL}$ given z can also be calculated in an analytical fashion.

The RBPF is known to be particularly effective and useful when nonlinear/non-Gaussian state variables can be clearly separated from linear/Gaussian state variables.

For the present application, Gaussian PDF's are assumed for all the uncertainties involved in the system, and clear state separation is not possible due to a complex nonlinear coupling between the system states. However, the state components involving high degree of nonlinearities can be separated from the augmented state vector in Equation (12). That is, the overall system states are divided into two parts, the target motion states ($\mathbf{x}_m$) and

parameter states ($\mathbf{x_p}$). Then, the EKF is used for estimating the motion state, and the PF for estimating the parameter states.

$$\mathbf{x} = \left[\begin{array}{c} \mathbf{x_m} \\ \hline \mathbf{x_p} \end{array}\right]$$
$$\mathbf{x_m} = \begin{bmatrix} X_T & Y_T & Z_T & \dot{X}_T & \dot{Y}_T & \dot{Z}_T \end{bmatrix}^T \tag{28}$$
$$\mathbf{x}_p = \begin{bmatrix} Z_1 & Z_2 & C_{Dm} & \omega \end{bmatrix}^T$$

This partition is based on the findings described in Section V, namely, the nonlinearities are more apparent for the parameter states associated with the harmonic spiraling motion than the motion states.

Additional simulations were carried out using the RBPF, and its performance has been compared to the EKF and UKF results. According to the simulation results, the RBPF with several hundred particles provides almost comparable or sometimes even better performance than the EKF and UKF. However, a real benefit of using the RBPF is the filter's robust performance under large initial uncertainties.

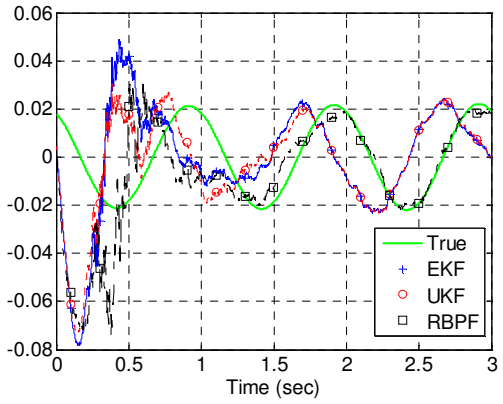

(a) Harmonic oscillation parameter (Z_1)

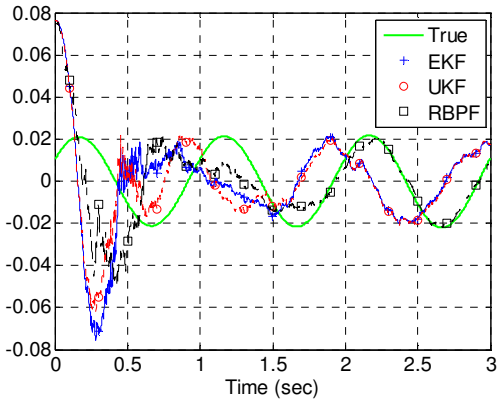

(b) Harmonic oscillation parameter (Z_2)

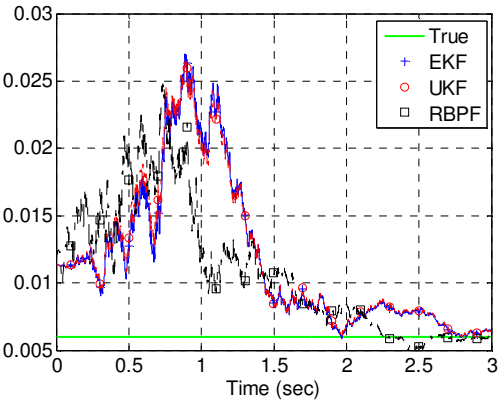

(c) Modified drag coefficient parameter

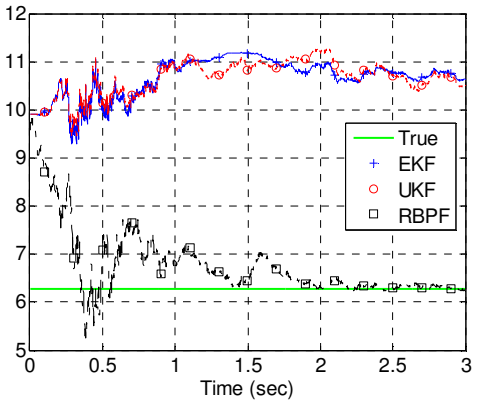

(d) Spiraling frequency parameter

Figure 9 Simulations under Large Initial Parameter Uncertainties

Figure 9 compares the simulations results for which much larger initial uncertainties were assumed for the parameter states. Most of the parameter state estimates by the EKF and UKF appear to get stuck in local minima and fails to converge. On the other hand, the RBPF successfully converges to the true parameter value. The computational cost of the RBPF is generally higher than the PF if the same number of particles is used. However, the RBPF generally needs much smaller number of particles than the standard PF.

VII. Concluding Remarks

Three nonlinear filtering techniques were applied to the problem of estimating the states and parameters of a ballistic target that undergoes spiraling motion during re-entry. Specifically, the EKF, UKF and PF were selected for the detailed performance analysis.

Based on extensive numerical simulation studies, the EKF and UKF are preferred over the PF for the current application. The EKF and UKF show satisfactory performance with excellent computational efficiency, as long as reasonable initial estimates are provided. On the other hand, it turned out that a standard PF is not an appropriate choice as an online recursive filtering method for this specific application because of the high dimensionality of the problem and the resulting prohibitive computational requirements.

Detailed performance comparisons between the EKF and UKF were also performed in the present research. The results revealed that the UKF outperforms the EKF in terms of filter stability and estimate accuracy at the price of minor increase in the computational effort.

Finally, the feasibility and utility of the RBPF were demonstrated to circumvent excessive computational requirements of the standard PF approach. The performance benefits in using the RBPF in terms of filter robustness against large initial uncertainties were shown.

Acknowledgments

This research was supported under MDA Contract No. HQ0006-05-C-7261.

References

[1] Farina, A., Ristic, B. and Benvenuti, D., "Tracking a Ballistic Target: Comparison of Several Nonlinear Filters," *IEEE Transactions on Aerospace and Electronic Systems*, Vol. 38, No. 3, pp. 854-867, July 2002.

[2] Saulson, B. G. and Chang, K., "Nonlinear Estimation Comparison for Ballistic Missile Tracking," *Optical Engineering*, Volume 43, pp. 1424-1438, June 2004.

[3] Zhao, Z., Chen, H., Chen, G., Kwan, C. and Li X. R., "Comparison of Several Ballistic Target Tracking Filters," *Proceedings of the 2006 American Control Conference*, Minneapolis, Minnesota, 2006.

[4] Ananthkrishnan, N., Raisinghani, S. C. and Pradeep, S., "Transient Resonance of Rolling Finned Projectiles," *Proceedings of the Institution of Mechanical Engineers Part G Journal of Aerospace Engineering*, pp. 97-103, 1999.

[5] Murphy, C. H., "Angular Motion of Spinning Almost-Symmetric Missiles," *Journal of Guidance and Control*, Vol. 2, pp. 504-510, 1979.

[6] Murphy, C. H., "Symmetric Missile Dynamic Instabilities," *Journal of Guidance and Control*, Vol. 4, pp. 464-471, 1980.

[7] Platus, D. H., "Ballistic Re-entry Vehicle Flight Dynamics," *Journal of Guidance and Control*, Vol. 5, pp. 4-16, 1982.

[8] Platus, D. H., "Missile and Spacecraft Coning Instabilities," *Journal of Guidance, Control, and Dynamics*, Vol. 17, pp. 1011-1018, 1994.

[9] Chadwick, W. R. and Zarchan, P., "Interception of Spiraling Ballistic Missiles," *Proceedings of the 1996 American Control Conference*, Seattle, Washington, 1996.

[10] Ohlmeyer, E. J., "Root-Mean-Square Miss Distance of Proportional Navigation Missile Against Sinusoidal Target," *Journal of Guidance, Control, and Dynamics*, Vol. 19, pp. 563-568, 1996.

[11] Zarchan, P. and Alpert, J., "Using Filter Banks to Improve Interceptor Performance Against Weaving Targets," *AIAA Guidnace, Navigation, and Control Conference*, Keystone, Colorado, 2006.

[12] Vaddi, S. S., Menon, P. K. and Ohlmeyer E. J., "Target State Estimation for Integrated Guidance-Control of Missiles," *AIAA Guidnace, Navigation, and Control Conference*, 2007.

[13] Khan, Z., Batch, T. and Dellaert F, "A Rao-Blackwellized Particle Filter for Eigen Tracking," *Proceedings of IEEE Computer Society Conference on Computer Vision and Pattern Recognition*, 2004.

[14] Schon, T. and Gustafsson, F. ".Marginalized Particle Filters for Mixed Linear/Nonlinear State-space Models," *IEEE Transactions on Signal Processing*, Vol. 53, No. 7, pp. 2279-2289, 2005.

[15] Gelb, A., *Applied Optimal Estimation*, The MIT Press, Cambridge, Massachusetts, 1974.

[16] Lewis, F. L., *Optimal Estimation with an Introduction to Stochastic Control Theory*, John Wiley & Sons, 1986.

[17] Julier, S. J. and Uhlmann, J. K., "A New Extension of the Kalman Filter to Nonlinear Systems," *International Symposium on Aerospace/Defense Sensing, Simulation and Control*, Orlando, Florida, 1997.

[18] Wan, E. A. and Merwe, R. van der, "The Unscented Kalman Filter for Nonlinear Estimation," *Proceedings of IEEE Symposium 2000*, Alberta, Canada , 2000.

[19] Langelaan, J. and Rock, S., "Towards Autonomous UAV Flights in Forests," *AIAA Guidance, Navigation and Control Conference*, San Francisco, CA, 2005.

[20] Thrun, S., Burgard, W. and Fox, D., *Probabilistic Robotics*, The MIT Press, Cambridge, Massachusetts, 2005.

[21] Arulampalam, M. S., Maskell, S., Gordon, N. and Clapp, T., ".A Tutorial on Particle Filters for Online Nonlinear/Non-Gaussian Bayesian Tracking," *IEEE Transactions on Signal Processing*, Vol. 50, No. 2, pp. 174-188, 2002.